PALEOGENOMICS

Denisovan DNA in Late Pleistocene sediments from Baishiya Karst Cave on the Tibetan Plateau

Dongju Zhang[1,2,3]*, Huan Xia[1], Fahu Chen[2,1], Bo Li[4,5]*, Viviane Slon[6], Ting Cheng[1], Ruowei Yang[7,8], Zenobia Jacobs[4,5], Qingyan Dai[7], Diyendo Massilani[6], Xuke Shen[1], Jian Wang[1,9], Xiaotian Feng[7], Peng Cao[7], Melinda A. Yang[10], Juanting Yao[1], Jishuai Yang[1], David B. Madsen[1,11], Yuanyuan Han[1], Wanjing Ping[6], Feng Liu[6], Charles Perreault[12,13], Xiaoshan Chen[1], Matthias Meyer[6], Janet Kelso[6], Svante Pääbo[6]*, Qiaomei Fu[7,8]*

A late Middle Pleistocene mandible from Baishiya Karst Cave (BKC) on the Tibetan Plateau has been inferred to be from a Denisovan, an Asian hominin related to Neanderthals, on the basis of an amino acid substitution in its collagen. Here we describe the stratigraphy, chronology, and mitochondrial DNA extracted from the sediments in BKC. We recover Denisovan mitochondrial DNA from sediments deposited ~100 thousand and ~60 thousand years ago (ka) and possibly as recently as ~45 ka. The long-term occupation of BKC by Denisovans suggests that they may have adapted to life at high altitudes and may have contributed such adaptations to modern humans on the Tibetan Plateau.

Denisovans are an extinct hominin group initially identified from a genome sequence determined from a fragment of a phalanx found at Denisova Cave in the Altai Mountains in southern Siberia (*1*–*3*). Subsequent analyses of the genome have shown that Denisovans diverged from Neanderthals ~400 thousand years ago (ka) (*4*) and that at least two distinct Denisovan populations mixed with ancestors of present-day Asians (*2*–*9*). Thus, they are assumed to have been widely dispersed across Asia. However, physical remains of Denisovans in Siberia have been restricted to a fragmentary phalanx (*1*), three teeth (*2*, *10*, *11*), and a cranial fragment (*12*), all of which were found at Denisova Cave.

Recently, half of a mandible from the Baishiya Karst Cave (BKC), Xiahe County, Gansu, China, dated to at least 160 ka, was identified to be of Denisovan origin (*13*). However, this identification of the Xiahe mandible as Denisovan is based on a single amino acid position and is therefore tenuous. Here we report the results of ongoing archaeological and chronological investigations and sedimentary DNA analyses from BKC. We find evidence for the long-term presence of Denisovans in BKC and provide stratigraphic and chronological context for their occupation in the cave.

BKC (35.45°N, 102.57°E, 3280 m above sea level) is a limestone cave located in the northeastern margin of the Tibetan Plateau (Fig. 1A and fig. S1A). In 2018 and 2019, three units that measured 1 m by 2 m (T1, T2, and T3) were plotted for excavation in the entrance chamber, which is about 60 m long, 8 m wide, and 5 m high (Fig. 1B and fig. S1, B and C) (*14*). The second unit (T2) exposed intact cultural strata that are truncated in the southeastern part of the trench by a large pit (H1) dug during the historical period (*14*), 780 to 700 calibrated years before present (where present is 1950 CE) (figs. S2 and S3 and table S3). Ten stratigraphic layers were identified mainly on the basis of sedimentary characteristics (figs. S2B and S3) (*14*). Most layers are poorly sorted, composed of a silt matrix with abundant angular clasts of autogenic limestone gravels. The latter originates from the reworking of eroded parent bedrock, sediments by colluviation, or spalling of material from the cave walls and roof (see details in the supplementary materials). Stone artifacts and animal fossils were recovered from all layers (figs. S11 and S12) (*14*). A total of 1310 stone artifacts and 579 animal bone fragments were recorded and collected. Preliminary analysis of the stone artifact assemblage suggests that they were made mostly from local metamorphic quartz sandstone and hornstone stream cobbles using a simple core and flake technology (fig. S11). Remains of small and medium-size animals, including gazelles, marmots, and foxes, dominate the fossil assemblage in layers 6 through 1, whereas large animals, such as rhinoceros, large bovids, and hyenas, dominate layers 10 through 7 (fig. S12).

We constructed a numerical chronology for the T2 sequence from optical dating of 12 sediment samples and radiocarbon dating of 14 bone fragments (Fig. 2, fig. S3, and tables S3, S9, and S10). The age estimates were used to develop a Bayesian model for the depositional chronology of the site and to provide an age framework for hominin occupation (Fig. 2 and table S12). Details of sample locations and collection, preparation, measurement, and data analysis procedures are provided, together with the measured and modeled ages and related data (*14*). The deposits in layers 10 to 4 have a stratigraphically coherent chronology, limited age variation within layers, and equivalent dose (D_e) distributions that show minimal evidence for mixing. Layer 10 accumulated between 190 ± 34 and 129 ± 20 ka (here and below, we give modeled age estimates and total uncertainties at 95.4% probability), followed by relatively fast accumulation of layers

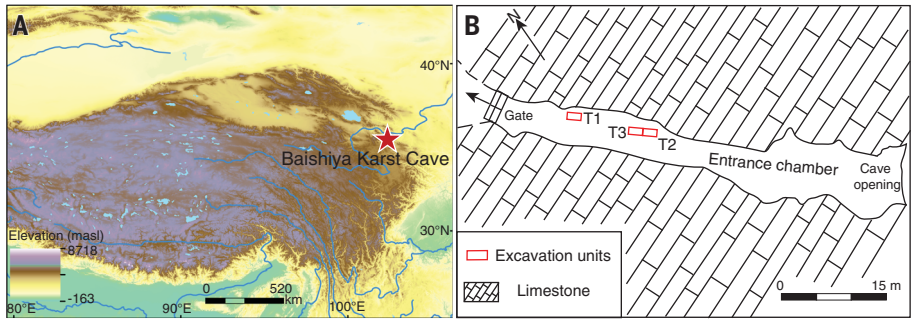

Fig. 1. Location of Baishiya Karst Cave on the Tibetan Plateau. (**A**) Regional map showing the location of the site. masl, meters above sea level. (**B**) Plan view of the entrance chamber and locations of excavation units (T1, T2, and T3). The gate separates the entrance chamber from other chambers farther inside the cave.

[1]Key Laboratory of Western China's Environmental Systems (Ministry of Education), College of Earth and Environmental Sciences, Lanzhou University, Lanzhou 730000, China. [2]Key Laboratory of Alpine Ecology (LAE), CAS Center for Excellence in Tibetan Plateau Earth Sciences and Institute of Tibetan Plateau Research, Chinese Academy of Sciences (CAS), Beijing 100101, China. [3]Frontier Center for Eco-environment and Climate Change in Pan-third Pole Regions, Lanzhou University, Lanzhou 730000, China. [4]Centre for Archaeological Science, School of Earth, Atmospheric and Life Sciences, University of Wollongong, Wollongong, New South Wales 2522, Australia. [5]Australian Research Council (ARC) Centre of Excellence for Australian Biodiversity and Heritage, University of Wollongong, Wollongong, New South Wales 2522, Australia. [6]Department of Evolutionary Genetics, Max Planck Institute for Evolutionary Anthropology, Leipzig 04103, Germany. [7]Key Laboratory of Vertebrate Evolution and Human Origins of Chinese Academy of Sciences, Institute of Vertebrate Paleontology and Paleoanthropology, CAS, Beijing 100044, China. [8]Center for Excellence in Life and Paleoenvironment, Chinese Academy of Sciences, Beijing 100044, China. [9]School of Earth Sciences, Lanzhou University, Lanzhou 730000, China. [10]Department of Biology, University of Richmond, Richmond, VA 23173, USA. [11]Department of Anthropology, University of Nevada–Reno, Reno, NV 89557, USA. [12]School of Human Evolution and Social Change, Arizona State University, Tempe, AZ 85281, USA. [13]Institute of Human Origins, Arizona State University, Tempe, AZ 85281, USA.
*Corresponding author. Email: djzhang@lzu.edu.cn (D.Z.); bli@uow.edu.au (B.L.); paabo@eva.mpg.de (S.P.); fuqiaomei@ivpp.ac.cn (Q.F.)

9 to 6 until 96 ± 5 ka. No age was obtained for layer 5. We modeled a time interval with a duration of 24 to 39 ka for layer 5. The sedimentary features of layer 5 (table S1) are indicative of a fluvial environment within BKC and may represent an erosional event that removed deposits dated to between ~100 and ~60 ka. Layer 4 was deposited from 66 ± 6 to 47 ± 2 ka. A depositional hiatus with a duration of ~7 to 18 ka was identified in the middle of layer 4 between ~60 and 50 ka, suggesting that sediments in layer 4 may have been deposited in two broad pulses. Layer 3 accumulated from 46 ± 2 ka 33 ± 1 ka, followed by layer 2 until 17 ± 12 ka. Layers 2 and 3 are more complex; radiocarbon ages vary considerably within a layer (table S3), and single-grain D_e values are broadly distributed (figs. S17 to S19 and S26).

To test whether ancient DNA was preserved in the cave, we extracted DNA (*15*) from eight sediment samples (100 to 250 mg each) collected from the middle of each layer (except layers 1 and 5) (Fig. 2A, fig. S3, and table S18). Aliquots of each extract were converted to DNA libraries and enriched for mammalian and human mitochondrial DNA (mtDNA) using probes for 242 mammalian mtDNAs (*15*) and for human mtDNA (*16*). For each library, the number of DNA fragments sequenced ranged from 0.07 to 1.7 million. From these, we obtained between 10 and 27,150 unique fragments mapping to mammalian mitochondrial genomes. All sampled layers, except layers 8 and 9, contained mammalian mtDNA. In layers 4, 6, 7, and 10, we detected DNA from animal species that have not been present in the area since ~10 ka, including extinct hyenas and rhinoceros (*17*), species for which bones were also identified in layer 10 (figs. S12 and S27). For all mammal sequences from all libraries corresponding to layers 2, 3, 4, 6, and 7 and four libraries from layer 10, the frequency of apparent terminal substitutions of cytosine (C) to thymine (T) at the 5′ end ranges from 10 to 65% (table S18), which is typical for ancient DNA. These results confirm that ancient DNA is preserved in the cave.

We then assessed whether ancient hominin DNA was present in each library by determining the frequency of apparent C→T substitutions in all hominin mtDNA fragments. The libraries from layers 2, 3, 4, and 7 have between 15.6 and 50% C→T terminal substitutions, indicating the presence of ancient hominin DNA (table S19). We thus prepared additional DNA extracts from layers 2, 3, 4, and 7 (table S18). To determine which hominin groups may have contributed mtDNA to these samples, we examined sequences for substitutions found to be specific to modern humans, Neanderthals, Denisovans, and a ~430,000-year-old hominin individual from Sima de los Huesos (Sima) (*18*) in phylogenetic analyses of mtDNAs as described (*14*, *19*).

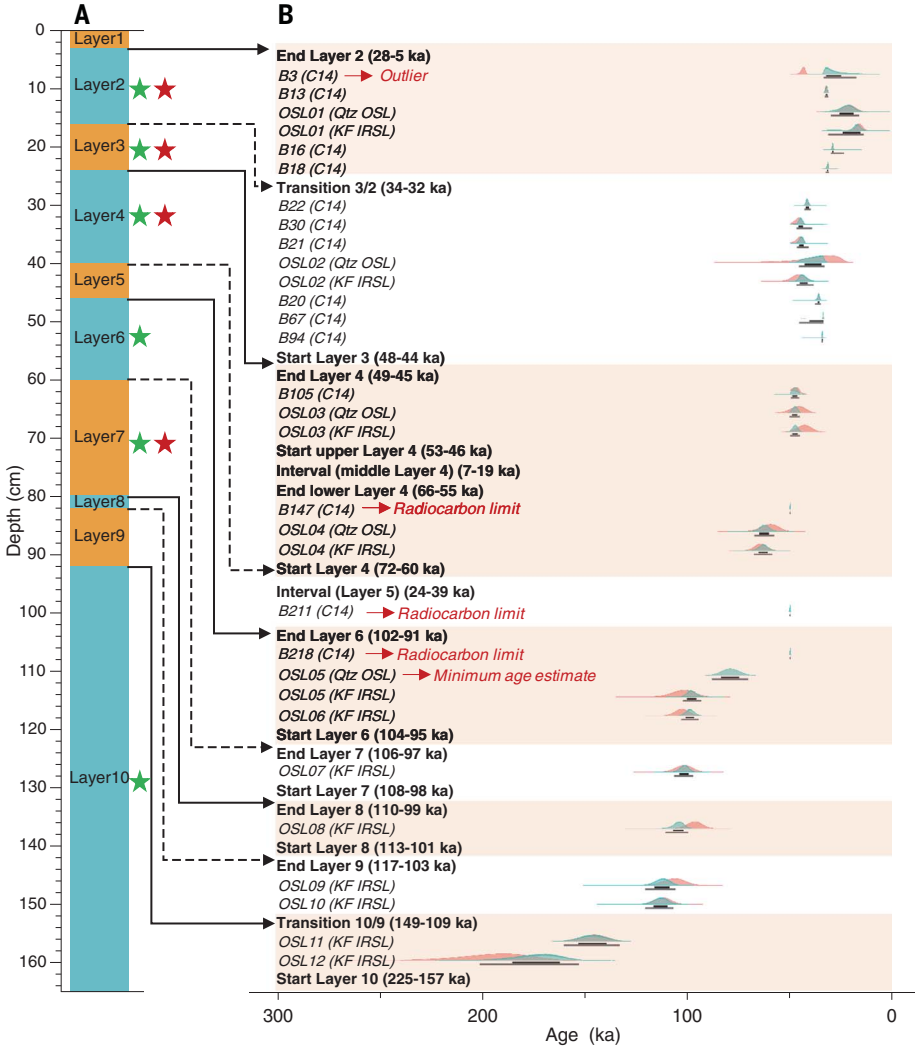

Fig. 2. Stratigraphy and dating results of T2. (**A**) Composite schematic stratigraphy of excavation area T2. The alternating colors are for illustration purposes only. The positions of sedimentary DNA samples from which Denisovan and animal DNA were found are shown as red stars and green stars, respectively. (**B**) Bayesian modeling results for all radiocarbon and optical ages. Red probability distributions represent the unmodeled ages (likelihoods), and green distributions represent the modeled ages (posterior probabilities). The narrow and wide bars beneath each distribution represent the 68.2 and 95.4% probability ranges of the modeled ages. Modeled ages for each layer boundary and phase and duration for each interval are given in parentheses (95.4% probability, random only errors).

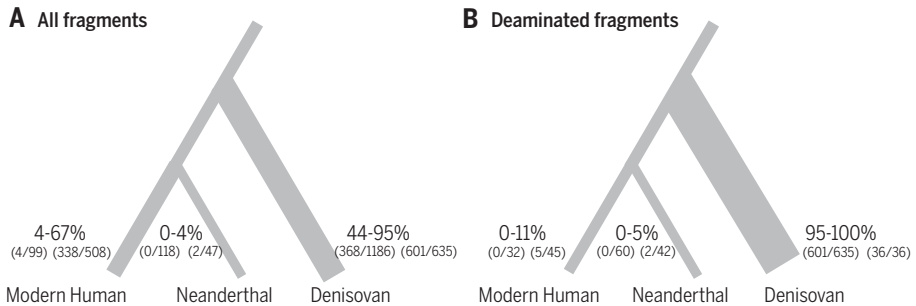

Fig. 3. Lineage inferences for layer 4. Using modern human, Neanderthal, and Denisovan branch-specific substitutions for all fragments (**A**) and deaminated fragments (**B**) from layer 4 for lineage inferences. Ranges for the percentage of lineage-matching sites for all libraries from layer 4 are given. The fractions give the absolute number of sequenced fragments carrying derived lineage-specific alleles over the total number of fragments covering positions where such alleles occur. The lineage inferences for layers 2, 3, and 7 are in fig. S28.

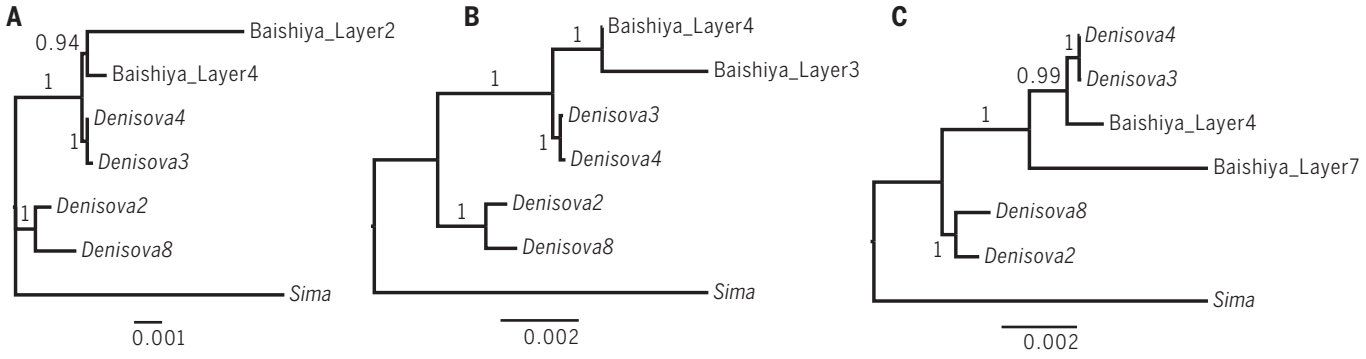

Fig. 4. mtDNA phylogenetic trees. mtDNA phylogenetic trees for sediment samples from layers 4 and 2 (**A**), layers 4 and 3 (**B**), or layers 4 and 7 (**C**) of the BKC as well as mtDNA from four Denisovans from Denisova Cave and a ~430,000-year-old hominin from Sima de los Huesos in Spain. Consensus sequences with deaminated fragments were used for BKC samples, except for layer 2 mtDNA, which is from all fragments from low contamination libraries and deaminated fragments from potentially contaminated libraries (see "decision" column in table S11). The phylogeny was estimated with a Bayesian approach under a general time reversible substitution model with a gamma distributed correction of sequence evolution.

From the 24 libraries, between 31% (368/1186) and 95% (601/635) of the mtDNA fragments that covered informative positions matched the Denisovan state (Fig. 3 and fig. S28), whereas 0 to 14% (1/7) matched the Neanderthal state (Fig. 3 and fig. S28), 0 to 3.7% (5/135) the Sima state (table S19), and 0 to 67% (338/508) the modern human state (Fig. 3 and fig. S28). Restricting the analysis to DNA fragments with first and last three C→T substitutions indicating cytosine deamination (Fig. 3 and fig. S28) decreased the proportion of fragments matching the modern human state to 0 to 43% (3/7) and increased the proportion matching the Denisovan state to 71 to 100%. To reduce the influence of modern human contamination, we restricted subsequent analyses to deaminated mtDNA fragments and excluded two DNA libraries in which modern human mtDNA fragments were slightly deaminated, albeit much less so than Denisovan mtDNA fragments (*14*).

By merging deaminated hominin mtDNA fragments from libraries for each layer, we arrive at an average mtDNA coverage for layers 2, 3, 4, and 7 of 0.37-fold, 1.5-fold, 40-fold, and 1.3-fold, respectively. DNA recovered from sediments may be derived from multiple different individuals, and this is the case at least in layer 4, where we have sufficient information to estimate the number of mtDNA fragments present (*14*). However, to gauge the average relationships of mtDNA in each layer, we called a consensus mtDNA sequence for each layer using positions covered by at least two different DNA fragments, excluding positions covered by only two fragments and where they differ. We also required that more than two-thirds of the fragments covering each position must carry an identical base at positions covered by more than two fragments (*18*). These sequences covered 7, 36, 99, and 26% of the mtDNA, respectively (table S15).

We then estimated phylogenetic trees using previously published mtDNA sequences from four Denisovans from Denisova Cave (Denisova 2, Denisova 3, Denisova 4, and Denisova 8) and the individual from Sima de los Huesos. The composite consensus mtDNA from layer 4 that is of comparatively high quality falls within the mtDNA variation of Denisovans, forming a clade with Denisova 3 and 4 to the exclusion of Denisova 2 and 8 (Fig. 4). When the consensus mtDNA sequences that are of lower quality are analyzed separately (Fig. 4), the mtDNA sequences from layers 2 and 3 form a clade with the layer 4 mtDNA, whereas the consensus layer 7 mtDNA diverges earlier from the lineage leading to Denisova 3 and 4. Thus, the mtDNA sequences from BKC form a clade (100% posterior support) with the mtDNA sequences for Denisova 3 and 4 (*20*, *21*). The depositional age for the lower part of layer 4 (~60 ka) (Fig. 2) is comparable to the date of Denisova 3 (76 to 52 ka) and Denisova 4 (84 to 55 ka) (*20*, *21*). Besides, the depositional age for layer 7 (108 to 97 ka) (Fig. 2) is older than those for Denisova 3 and 4 but younger than the ages for Denisova 2 (194 to 122 ka) and Denisova 8 (136 to 105 ka) (*20*, *21*). Although Denisovan mtDNA is present in layers 3 and 2, it is tenuous to associate them to their corresponding depositional ages (~30 to 50 ka), given the reworked nature of the layers. Therefore, whether the BKC Denisovans had survived until the arrival of modern humans on the Tibetan Plateau by 30 to 40 ka (*22*) remains an open question.

In conclusion, the stratigraphic, chronological, and sedimentary DNA results presented show that Denisovans occupied BKC at ~100 and ~60 ka. This confirms that Denisovans were widely distributed in Asia during the Late Pleistocene. Together with the older Xiahe mandible, this evidence suggests a long occupation of the Tibetan Plateau by individuals who may have become adapted to the high-altitude environment. The genetic adaptations to high altitudes seen in modern Tibetans could be associated with a haplotype introgressed from Denisovans (*23*) that perhaps evolved during the extended occupation of this high-altitude environment by Denisovans. Deeper investigations at BKC and other Paleolithic sites in a broader region surrounding the Tibetan Plateau may help to understand the relationship and evolution of Denisovans, modern humans, and possible other archaic humans in East Asia.

REFERENCES AND NOTES

1. J. Krause *et al.*, *Nature* **464**, 894–897 (2010).
2. D. Reich *et al.*, *Nature* **468**, 1053–1060 (2010).
3. M. Meyer *et al.*, *Science* **338**, 222–226 (2012).
4. K. Prüfer *et al.*, *Nature* **505**, 43–49 (2014).
5. D. Reich *et al.*, *Am. J. Hum. Genet.* **89**, 516–528 (2011).
6. P. Qin, M. Stoneking, *Mol. Biol. Evol.* **32**, 2665–2674 (2015).
7. S. Sankararaman, S. Mallick, N. Patterson, D. Reich, *Curr. Biol.* **26**, 1241–1247 (2016).
8. B. Vernot *et al.*, *Science* **352**, 235–239 (2016).
9. S. R. Browning, B. L. Browning, Y. Zhou, S. Tucci, J. M. Akey, *Cell* **173**, 53–61.e9 (2018).
10. S. Sawyer *et al.*, *Proc. Natl. Acad. Sci. U.S.A.* **112**, 15696–15700 (2015).
11. V. Slon *et al.*, *Sci. Adv.* **3**, e1700186 (2017).
12. B. Viola *et al.*, *Am. J. Phys. Anthropol.* **168**, 258 (2019).
13. F. Chen *et al.*, *Nature* **569**, 409–412 (2019).
14. Materials and methods are available as supplementary materials.
15. V. Slon *et al.*, *Science* **356**, 605–608 (2017).
16. Q. Fu *et al.*, *Proc. Natl. Acad. Sci. U.S.A.* **110**, 2223–2227 (2013).
17. G. Zong, W. Chen, X. Huang, Q. Xu, *Cenozoic Mammals and Environment of Hengduan Mountains Region* (China Ocean Press, 1996).
18. M. Meyer *et al.*, *Nature* **505**, 403–406 (2014).
19. M. Meyer *et al.*, *Nature* **531**, 504–507 (2016).
20. K. Douka *et al.*, *Nature* **565**, 640–644 (2019).
21. Z. Jacobs *et al.*, *Nature* **565**, 594–599 (2019).
22. X. L. Zhang *et al.*, *Science* **362**, 1049–1051 (2018).
23. E. Huerta-Sánchez *et al.*, *Nature* **512**, 194–197 (2014).
24. X. Xu *et al.*, *Nucleic Acids Res.* **46**, D14–D20 (2018).

ACKNOWLEDGMENTS

We thank G. Dong, Z. Wang, J. Brantingham, and D. Rhode for participating in early investigation of BKC; Z. Li and D. Lin for help in the interpretation of sedimentary data; M. Qiu for taking photos of the stone artifacts and bones; and S. Pang, Z. Jiang, and Z. Jia for

measuring the cave. We are grateful to the support of National Cultural Heritage Administration of China, Provincial Cultural Heritage Administration of Gansu, Gansu Provincial Archaeological Institute, and local government for our archaeological excavation in BKC. We are also grateful to the support from the Baishiya Temple and the local residents in Ganjia town. **Funding:** This study was funded by the Second Tibetan Plateau Scientific Expedition and Research Program (STEP) (2019QZKK0601) and the Strategic Priority Research Program (XDB26000000, XDA20040000) of CAS; NSFC (41771225) to D.Z.; NSFC (91731303, 41925009, 41672021, 41630102), Tencent Foundation through the EXPLORER PRIZE, and "Research on the roots of Chinese civilization" of Zhengzhou University (XKZDJC202006) to Q.F.; The Strategic Innovation Fund of the Max Planck Society to S.P.; and Australian Research Council Future Fellowships to B.L. (FT140100384) and Z.J. (FT150100138). **Author contributions:** D.Z. and F.C. designed the study. D.Z., F.C., H.X., T.C., X.S., J.W., J. Yao, J. Yang, D.B.M., C.P., Y.H., and X.C. carried out field investigation, excavated the site, and carried out sampling processes. D.Z., F.C., H.X., B.L., D.B.M., and C.P. conducted stratigraphic and taphonomy analysis. B.L., Z.J., H.X., and T.C. performed the OSL and radiocarbon dating. Q.F., R.Y., Q.D., X.F., P.C., W.P., and F.L. performed the ancient DNA experiments and analysis. S.P., M.M., J.K., V.S., and D.M. helped for discussing and interpreting the genetic data. D.Z., Q.F., S.P., B.L., M.A.Y., Z.J., and F.C. wrote the paper with contributions from all authors. **Competing interests:** The authors declare no competing interests; **Data and materials availability:** All relevant data are available in the main text or the accompanying supplementary materials. The new mitochondrial consensus files reported in this paper have been deposited in the Genome Warehouse in National Genomics Data Center (*24*), Beijing Institute of Genomics (China National Center for Bioinformation), Chinese Academy of Sciences, under accession number PRJCA002765, which is publicly accessible at https://bigd.big.ac.cn/gwh. Artifacts and animal fossils referred to in this study are curated in Lanzhou University.

SUPPLEMENTARY MATERIALS

science.sciencemag.org/content/370/6516/584/suppl/DC1
Materials and Methods
Figs. S1 to S29
Tables S1 to S19
References (*25*–*127*)
MDAR Reproducibility Checklist

View/request a protocol for this paper from *Bio-protocol*.

27 April 2020; accepted 10 September 2020
10.1126/science.abb6320

MAGNETISM

Metal-organic magnets with large coercivity and ordering temperatures up to 242°C

Panagiota Perlepe[1,2], Itziar Oyarzabal[1,3]*, Aaron Mailman[4], Morgane Yquel[1,2], Mikhail Platunov[5]†, Iurii Dovgaliuk[6]‡, Mathieu Rouzières[1], Philippe Négrier[7], Denise Mondieig[7], Elizaveta A. Suturina[8], Marie-Anne Dourges[9], Sébastien Bonhommeau[9], Rebecca A. Musgrave[1], Kasper S. Pedersen[1,10], Dmitry Chernyshov[6], Fabrice Wilhelm[5], Andrei Rogalev[5], Corine Mathonière[2], Rodolphe Clérac[1]*

Magnets derived from inorganic materials (e.g., oxides, rare-earth–based, and intermetallic compounds) are key components of modern technological applications. Despite considerable success in a broad range of applications, these inorganic magnets suffer several drawbacks, including energetically expensive fabrication, limited availability of certain constituent elements, high density, and poor scope for chemical tunability. A promising design strategy for next-generation magnets relies on the versatile coordination chemistry of abundant metal ions and inexpensive organic ligands. Following this approach, we report the general, simple, and efficient synthesis of lightweight, molecule-based magnets by postsynthetic reduction of preassembled coordination networks that incorporate chromium metal ions and pyrazine building blocks. The resulting metal-organic ferrimagnets feature critical temperatures up to 242°C and a 7500-oersted room-temperature coercivity.

Magnets that operate at room temperature are usually pure metals, metal oxides, or intermetallic compounds, and they have applications in numerous aspects of our daily lives. For example, magnets are key components in data processing and storage devices, are commonly used in electrical motors that power most household appliances, and are essential in renewable energy technologies (*1*). Despite their extensive use and tremendous success in technological applications, conventional magnets present several drawbacks, such as energetically expensive fabrication (e.g., for SmCo and AlNiCo) and limited availability of key component elements (e.g., in the rare-earth–based magnets NdFeB and SmCo). Over the last three decades, various approaches have been developed to address these limitations and to target next-generation magnets. One particularly appealing strategy relies on the rational assembly of molecular building blocks, such as organic ligands and paramagnetic metal ions. These molecule-based materials exhibit behavior similar to that of traditional magnets; however, unlike the exclusively inorganic examples, they benefit from the synthetic and postsynthetic versatility that results from the molecular and coordination chemistries, which allow precise tailoring and optimization of their properties (*2*–*4*). This synthetic approach has already led to a vast number of systems with peculiar magnetic behaviors, several of which have no counterpart in inorganic materials. Among these molecule-based magnets are discrete high-spin molecules known as single-molecule magnets (SMMs) (*5*, *6*), one-dimensional (1D) magnets (single-chain magnets) (*7*), and 2D and 3D networks exhibiting magnetically ordered phases (*8*). By separating magnetic metal ions with organic ligands, these molecule-based materials feature remarkably low densities (~1 g cm^{-3}) compared with those of exclusively inorganic materials (generally >5 g cm^{-3}). Although state-of-the-art inorganic magnets are indispensable because of their high maximum energy product [i.e., high magnetic density (*9*)], complementary molecule-based magnetic materials will be of great relevance to emergent magnetoelectronic, magnetic sensing, and recording technologies as a result of their low density. However, most of these molecule-based materials suffer from low operating temperatures, which has precluded technological application.

To raise the operating temperature of molecule-based magnets, closed-shell ligands have been replaced by radicals to link paramagnetic metal ions in 2D or 3D coordination networks (*8*). The presence of a radical's spin leads to particularly strong magnetic interactions with the metal centers, which can be controlled by the chemical identity of the organic radical and metal ion, and the overlap of their magnetic orbitals containing an unpaired electron (*8*, *10*, *11*). This methodology is exemplified by the pioneering work of J. S. Miller on a family of magnets incorporating paramagnetic metal ions and organic radical species such as the tetracyanoethylene radical ($[TCNE]^{\bullet-}$) (*12*). In these systems, the strong magnetic coupling between spins localized in the metal 3d orbitals and those of the radicals result in magnetically ordered phases with critical temperatures (T_C) as high as 400 K ($V[TCNE]_x$ where $x \sim 2$) (*13*). Apart from displaying the current record T_C value measured for a molecule-based magnet, $V[TCNE]_x$ has also shed light on the applicability of molecule-based, lightweight magnets

[1]Université de Bordeaux, CNRS, Centre de Recherche Paul Pascal, UMR 5031, F-33600 Pessac, France. [2]Université de Bordeaux, CNRS, Bordeaux INP, ICMCB, UMR 5026, F-33600 Pessac, France. [3]Chemistry Faculty, University of the Basque Country, UPV/EHU, 20018 Donostia-San Sebastián, Spain. [4]Department of Chemistry, University of Jyväskylä, FI-40014 Jyväskylä, Finland. [5]ESRF-The European Synchrotron, CS 40220, F-38043 Grenoble Cedex 9, France. [6]Swiss-Norwegian Beamlines at the European Synchrotron Radiation Facility, F-38000 Grenoble, France. [7]Université de Bordeaux, CNRS, Laboratoire Ondes et Matière d'Aquitaine, UMR 5798, F-33400 Talence, France. [8]Department of Chemistry, University of Bath, Claverton Down, Bath BA2 7AY, UK. [9]Université de Bordeaux, CNRS, Bordeaux INP, ISM, UMR 5255, F-33400 Talence, France. [10]Department of Chemistry, Technical University of Denmark, DK-2800 Kongens Lyngby, Denmark.
***Corresponding author. Email: itziar.oyarzabal@ehu.eus (I.O.); clerac@crpp-bordeaux.cnrs.fr (R.C.)**
†Present address: Kirensky Institute of Physics, Federal Research Center KSC SB RAS, 660036 Krasnoyarsk, Russia.
‡Present address: Institut des Matériaux Poreux de Paris, UMR 8004 CNRS, Ecole Normale Supérieure, Ecole Supérieure de Physique et de Chimie Industrielles de Paris, PSL Université, 75005 Paris, France.